Brain Structure and Function (2018) 223:3875–3887
https://doi.org/10.1007/s00429-018-1729-7

ORIGINAL ARTICLE

PLP1 and *CNTN1* gene variation modulates the microstructure of human white matter in the corpus callosum

Catrona Anderson[1,2] · Wanda M. Gerding[3] · Christoph Fraenz[2] · Caroline Schlüter[2] · Patrick Friedrich[2] · Maximilian Raane[4] · Larissa Arning[3] · Jörg T. Epplen[3,4] · Onur Güntürkün[2] · Christian Beste[5,6] · Erhan Genç[2] · Sebastian Ocklenburg[2]

Received: 4 December 2017 / Accepted: 3 August 2018 / Published online: 9 August 2018

Abstract

The corpus callosum is the brain's largest commissural fiber tract and is crucial for interhemispheric integration of neural information. Despite the high relevance of the corpus callosum for several cognitive systems, the molecular determinants of callosal microstructure are largely unknown. Recently, it was shown that genetic variations in the myelin-related proteolipid 1 gene *PLP1* and the axon guidance related contactin 1 gene *CNTN1* were associated with differences in interhemispheric integration at the behavioral level. Here, we used an innovative new diffusion neuroimaging technique called neurite orientation dispersion and density imaging (NODDI) to quantify axonal morphology in subsections of the corpus callosum and link them to genetic variation in *PLP1* and *CNTN1*. In a cohort of 263 healthy human adults, we found that polymorphisms in both *PLP1* and *CNTN1* were significantly associated with callosal microstructure. Importantly, we found a double dissociation between gene function and neuroimaging variables. Our results suggest that genetic variation in the myelin-related gene *PLP1* impacts white matter microstructure in the corpus callosum, possibly by affecting myelin structure. In contrast, genetic variation in the axon guidance related gene *CNTN1* impacts axon density in the corpus callosum. These findings suggest that *PLP1* and *CNTN1* gene variations modulate specific aspects of callosal microstructure that are in line with their gene function.

Keywords Myelin · Corpus callosum · *PLP1* · *CNTN1* · White matter · NODDI

Introduction

White matter comprises about 30–40% of the human cerebral cortex (Ge et al. 2002). In recent years, neuroscience has acknowledged that white matter plays an important role in cognition, especially within a network-driven understanding of human cognition. For example, reduced white matter in aging brains is associated with impaired executive functioning (DeCarli et al. 1995), impaired spatial and verbal abilities (Skoog et al. 1996),

Catrona Anderson, Wanda M. Gerding, Erhan Genç and Sebastian Ocklenburg contributed equally to the manuscript.

Electronic supplementary material The online version of this article (https://doi.org/10.1007/s00429-018-1729-7) contains supplementary material, which is available to authorized users.

✉ Catrona Anderson
cat.anderson@otago.ac.nz

[1] Department of Psychology, University of Otago, P. O. Box 56, Dunedin, New Zealand

[2] Institute of Cognitive Neuroscience, Biopsychology, Department of Psychology, Ruhr-University Bochum, Bochum, Germany

[3] Department of Human Genetics, Ruhr-University Bochum, Bochum, Germany

[4] Faculty of Health, ZBAF, University of Witten/Herdecke, Witten, Germany

[5] Cognitive Neurophysiology, Department of Child and Adolescent Psychiatry, Faculty of Medicine, TU Dresden, Dresden, Germany

[6] Experimental Neurobiology, National Institute of Mental Health, Topolova 748, 25067 Klecany, Czech Republic

and lower performance IQ (Garde et al. 2000). Therefore, it appears that white matter is essential for normal cognitive functioning.

There are three main types of white matter pathways. Association pathways, such as the arcuate fasciculus, connect different brain areas within one hemisphere. Projection pathways, such as the corticospinal tract, connect cortical areas to subcortical networks. The third type of white matter pathways is commissural pathways, such as the corpus callosum, which connect areas between the two hemispheres (Schmahmann et al. 2008). In particular, commissural pathways have been the focus of research concerning the impact of white matter structures on human cognition, as they are critical in ensuring that the left- and right-hemispheric subsections of integrated neural networks work together smoothly (Suárez et al. 2014; van der Knaap and van der Ham 2011).

The largest commissural pathway in the human brain is the corpus callosum, consisting of approximately 200 million fibers (Fabri et al. 2014). While the corpus callosum consists of some heterotopic interconnections, in which different areas in the two hemispheres are connected, most interconnections are homotopic, in which the same areas in the left and right hemisphere are connected (Clarke and Zaidel 1994). Therefore, the corpus callosum is crucial for the bilateral integration of motor, sensory, and higher-order cognitive networks in humans (Suárez et al. 2014).

To perform this integration of neuronal information, a high transmission speed of neuronal information is pivotal. The transmission speed of information along callosal axons is dependent on two main factors. First, axon diameter determines transmission speed, with thicker axons showing higher conduction velocity (Caminiti et al. 2009). Second, axon myelination also determines transmission speed, with myelinated axons increasing conduction over unmyelinated axons (van der Knaap et al. 2005). Importantly, the corpus callosum is not one uniform structure, but instead is organized according to an anterior–posterior topography gradient (Schmahmann et al. 2008). Anterior parts of the corpus callosum have been shown to connect anterior parts of the cortex, and posterior callosal fibers to areas in the posterior cortex (Hofer and Frahm 2006).

Myelination also differs between parts of the corpus callosum. Posterior parts of the corpus callosum, which connect sensory areas such as the occipital lobe and auditory network, tend to have more myelinated axons (Aboitiz et al. 1992a, b). On the other hand, anterior parts of the corpus callosum, which connect frontal areas of the brain, tend to have less myelinated axons (Aboitiz et al. 1992). These differences in subsection myelination have been suggested to reflect a need for higher conduction velocity in sensory areas, compared to frontal areas (Westerhausen and Hugdahl 2008).

Myelin plays a critical role in interhemispheric transmission of information. Therefore, we have recently suggested that to investigate the molecular basis of interhemispheric integration, research should look to variation in specific genes involved in myelin sheath formation and the axon ensheathment process (Ocklenburg et al. 2017). We previously genotyped a cohort of 453 healthy adults for 18 single nucleotide polymorphisms (SNPs) in six myelin-related candidate genes (*PLP1, GPM6A, MOG, MBP, CNTN1*, and *MOBP*). Interhemispheric integration was tested using the Banich–Belger task (Banich and Belger 1990), a commonly used behavioral task to assess this important function of the corpus callosum. Interestingly, the results of our previous study indicated that specific sequence variations in *PLP1* and *CNTN1* were associated with interindividual differences in interhemispheric integration in the Banich–Belger task (Ocklenburg et al. 2017).

PLP1 encodes the proteolipid protein 1, which serves as the predominant component in myelin, and constitutes around 80% of myelin protein mass along with another major myelin protein, myelin basic protein *MBP* (Boiko and Winckler 2006). *PLP1* is directly relevant for the development of the human corpus callosum, since mutations in *PLP1* can lead to atrophy of the corpus callosum (Sarret et al. 2016). *CNTN1* encodes contactin 1, a protein that is associated with ogliodendrocyte differentiation, and axon guidance and formation (Czopka et al. 2010). It has been shown to modulate axon connections and neurogenesis during central nervous system development (Bizzoca et al. 2012).

While our previous results strongly suggest that *PLP1* and *CNTN1* are relevant for interhemispheric integration on the behavioral level, possibly by modulating corpus callosum function, the actual impact of genetic variation of these genes on corpus callosum microstructure is still unclear. However, revealing this relationship would be a critical step in establishing the relevance of these genes for corpus callosum development. Thus, the present study is the first neurogenetic study to link *PLP1* and *CNTN1* gene variation to neuroimaging parameters of corpus callosum microstructure.

Conventional imaging methods such as diffusion tensor imaging (DTI) allow for in-vivo tractography of specific fiber tracts (Behrens et al. 2007) as well as the microstructural quantification of white matter via means of fractional anisotropy (FA; Le Bihan 2003; Pierpaoli and Basser 1996). FA in white matter is thought to reflect myelin, axon diameter and packing density, axon permeability, and fiber geometry (Beaulieu 2002; Mädler et al. 2008; Mori and Zhang 2006; Zatorre et al. 2012) and is thus seen as a measure of microstructural integrity (Genç et al. 2015; Zatorre et al. 2012). However, the function of the corpus callosum is determined by both its myelination and structural properties

of its neurites such as axon geometry. Thus, conventional DTI might not be the optimal phenotype in neurogenetic studies investigating genetic associations with corpus callosum structure, as it does not measure neurite structure. A better neuroimaging technique to use as a phenotype in such studies is neurite orientation dispersion and density imaging (NODDI), as it allows for the assessment of FA and also offers a novel way to quantify neurite morphology in white matter, that is, both axons and dendrites. NODDI was recently used to estimate diffusion markers of neurite density and orientation dispersion by in-vivo measurements in humans (Genç et al. 2018; Zhang et al. 2012). NODDI uses a multi-shell high-angular-resolution diffusion imaging protocol and features a three-compartment model distinguishing intra-neurite, extra-neurite, and cerebrospinal fluid (CSF) environments. Furthermore, NODDI is based on a diffusion model, which was successfully validated by histological examinations utilizing staining methods in the gray and white matter of rats and ferrets (Jespersen et al. 2010, 2012). NODDI yields three dependent measures: INVF, ODI, and ISO. Intra-neurite volume fraction (INVF) is a measure of neurite density, and represents the amount of symmetric diffusion caused by the restriction of water molecules within the membranes of neurites (Jespersen et al. 2010, 2012; Zhang et al. 2012). In contrast, orientation dispersion (ODI) is a measure of dendritic arborization, and isotropic volume fraction (ISO) reflects the amount of isotropic diffusion with Gaussian properties likely to be found in the cerebrospinal fluid. As the corpus callosum comprised of axons, but not dendrites, NODDI is used to specifically measure axonal density and orientation dispersion, rather than the neurite as a whole. NODDI has been used to detect white matter microstructural deficits in multiple sclerosis patients. Grussu et al. (2017) reported that neurite density obtained from NODDI significantly matched neurite density, orientation dispersion, and myelin density obtained from histological samples. Moreover, Grussu et al. (2017) also found that NODDI neurite dispersion matched histological neurite dispersion. These findings indicate that NODDI metrics are a valid measure of white matter microstructure as they closely reflect their histological conditions.

The aim of the current study was to examine the effects of genetic variation in the *PLP1* and *CNTN1* myelin-related genes on the microstructure of the corpus callosum as assessed with FA and the three NODDI measures, INVF, ODI, and ISO. As myelination and axon density differ between different subsections of the corpus callosum (Aboitiz et al. 1992a, b), we specifically assessed five subsegments of the corpus callosum, following the commonly used classification scheme by Hofer and Frahm (2006). As *PLP1* encodes for the proteolipid protein 1, the predominant component of myelin, we hypothesize that the genetic variation in *PLP1* should be linked to differences in FA, as this measure encodes microstructural integrity of white matter and has been at least partly linked to myelin structure. In contrast, *CNTN1* has been linked to axon formation and guidance. Thus, we expect genetic variation in *CNTN1* to be associated with axonal density differences between subsections of the corpus callosum as reflected by INVF.

Methods

Participants

Overall, we tested a cohort of 263 healthy adults (135 males and 128 females). Participants ranged in age from 18 to 69 years (mean age 25.2 years) and were mostly university students. All participants were of Caucasian descent for at least two generations, the majority of which were German. Participants were genetically unrelated to each other, as measured via self-reports. The majority of participants were right-handed (240 right-handers and 23 left-handers) as determined by the Edinburgh Handedness Inventory (Oldfield 1971). All participants gave informed written consent and were treated in accordance with the Declaration of Helsinki. The study was approved by the ethics committee of the medical faculty, Ruhr-University Bochum.

Genotyping

Oral mucosa samples were collected with buccal swabs from all participants. DNA isolation of the exfoliated cells was performed using the QIAamp DNA kit (Qiagen GmbH, Hilden, Germany). To genotype selected genes, polymerase chain reaction (PCR) and restriction fragment length polymorphism (RFLP) was used. Further details and primer sequences are available upon request. Based on our previous results (Ocklenburg et al. 2017), in which we found associations between myelin gene variation and interhemispheric integration, we focused on genotyping three different SNPs: *CNTN1* rs1056019, a synonymous exchange N472N located in exon 11; and two in *PLP1*, rs1126707, a synonymous exchange D203D in exon 11, and rs521895 located in intron 3.

Neuroimaging

Acquisition of imaging data

All imaging data were acquired at the Bergmannsheil hospital in Bochum, Germany, using a 3 T Philips Achieva scanner (Best, The Netherlands) with a 32-channel head coil.

Anatomical imaging For the purpose of segmenting brain scans into gray and white matter sections as well as for the

identification of anatomical landmarks, a T1-weighted high-resolution anatomical image was acquired (MP-RAGE, TR = 8.2 ms, TE = 3.7 ms, flip angle = 8°, 220 slices, matrix size = 240 × 240, resolution = 1 × 1 × 1 mm). The acquisition time of the anatomical image was 6 min.

Diffusion-weighted imaging For the analysis of NODDI coefficients, diffusion-weighted images were acquired using echo planar imaging (TR = 7652 ms, TE = 87 ms, flip angle = 90°, 60 slices, matrix size = 112 × 112, resolution = 2 × 2 × 2 mm). Diffusion weighting was based on a multi-shell, high-angular resolution scheme consisting of diffusion-weighted images for *b*-values of 1000, 1800, and 2500 s/mm^2, respectively, applied along 20, 40, and 60 uniformly distributed directions. All diffusion directions within and between shells were generated orthogonal to each other using the MASSIVE toolbox (Froeling et al. 2017). Additionally, eight data sets with no diffusion weighting ($b = 0$ s/mm^2) were acquired as an anatomical reference for motion correction and computation of NODDI coefficients. The acquisition time of the diffusion-weighted images was 18 min.

Analysis of imaging data

Analysis of anatomical data We used published surface-based methods in FreeSurfer (http://surfer.nmr.mgh.harvard.edu, version 5.3.0) to reconstruct the cortical surfaces of the T1-weighted images (see Fig. 1, top-left). The details of this procedure have been described elsewhere (Dale et al. 1999; Fischl et al. 1999). The automatic reconstruction steps included skull stripping, gray and white matter segmentation, as well as reconstruction and inflation of the cortical surface. These processing steps were performed for each participant individually. After preprocessing, each segmentation was quality-controlled slice by slice. Inaccuracies for the automatic steps were corrected by manual editing if necessary. The parcellation of the corpus callosum was done using an automatic segmentation procedure implemented in FreeSurfer (Rosas et al. 2010). The parcellation scheme was based on the Hofer and Frahm (2006) approach and was

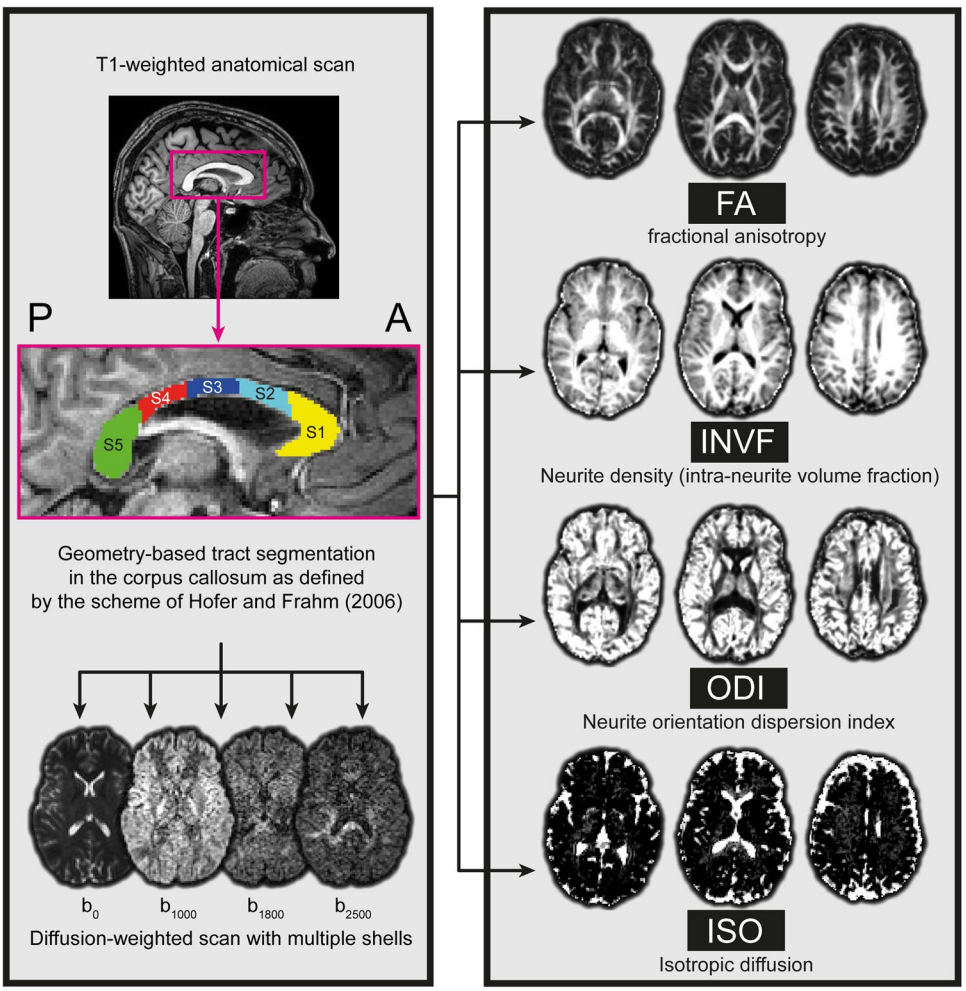

Fig. 1 Schematic description of the geometry-based tract segmentation in the corpus callosum and estimation of diffusion properties. Geometry-based tract segmentation of the corpus callosum via T1-weighted images in FreeSurfer (top-left). As defined by the scheme of (Hofer and Frahm 2006), the whole corpus callosum was divided into five subsections from anterior to posterior along the *y*-axis (middle-left): the five callosal subsections were defined as: the anterior sixth section (S1, yellow), the anterior half minus the anterior sixth section (S2, light-blue), the posterior half minus the posterior third section (S3, blue), the posterior third minus the posterior one-fourth section (S4, red), and the posterior one-fourth section (S5, green). The callosal subsections were linearly transformed into the native space of the diffusion-weighted NODDI images (bottom-left) and different microstructural measures (FA, INVF, ODI, ISO) were computed (right-panel). The following abbreviations are used: P, posterior; A, anterior

utilized to divide the corpus callosum into five subsections along the anterior to posterior *y*-axis (see Fig. 1, middle-left). The five callosal subsections were defined as: the anterior sixth section (S1), the anterior half minus the anterior sixth section (S2), the posterior half minus the posterior third section (S3), the posterior third minus the posterior one-fourth section (S4), and the posterior one-fourth section (S5). In a final step, each callosal subsection yielded by the parcellation algorithm was linearly transformed into the native space of the diffusion-weighted images (see Fig. 1, bottom-left). The transformed subsection served as anatomical landmarks from which NODDI coefficients were extracted.

Analysis of diffusion data Diffusion images were preprocessed using FDT (FMRIB's Diffusion Toolbox) as implemented in FSL version 5.0.7. Preprocessing steps included a correction for eddy currents and head motion as well as a correction of the gradient direction for each volume using the rotation parameters emerged from head motion. NODDI coefficients were computed using the AMICO toolbox (Daducci et al. 2015). The AMICO approach is based on a convex optimization procedure which converts the non-linear fitting into a linear optimization problem (Daducci et al. 2015). This framework allows robust estimation of multiple fiber populations as well as microstructural NODDI indices by dramatically reducing processing time (Sepehrband et al. 2016; Tariq et al. 2016). Data analysis with NODDI can be applied to cortical regions as well as white matter structures. The technique is based on a two-level approach and features a three-compartment model distinguishing intra-neurite, extra-neurite, and CSF environments. First, the diffusion signal obtained by the multi-shell high-angular-resolution imaging protocol is used to determine the proportion of free moving water within each voxel (Billiet et al. 2015; Daducci et al. 2015; Jespersen et al. 2010, 2012; Zhang et al. 2012). This ratio is termed isotropic volume fraction (ISO) and reflects the amount of isotropic diffusion with Gaussian properties likely to be found in the cerebrospinal fluid of gray and white matter regions (see Fig. 1, bottom-right). Second, the remaining portion of the diffusion signal is divided into the intra-neurite volume fraction (INVF) and the extra-neurite volume fraction. Here by definition, the two volume fractions representing intra- and extra-neurite diffusion complement each other and add up to 1 (Jespersen et al. 2010, 2012; Zhang et al. 2012). INVF represents the amount of stick-like or cylindrically symmetric diffusion that is created when water molecules are restricted by the membranes of neurites. In white matter structures, this kind of diffusion is likely to resemble the proportion of axons (see Fig. 1, middle-right). In gray matter regions, it serves as an indicator of dendrites and axons forming the neuropil. Extra-neurite volume fraction is based on hindered diffusion within extra-neurite environments, which are usually occupied by various types of glial cells in white matter structures, and both neurons and glial cells in gray matter regions (Jespersen et al. 2010, 2012; Zhang et al. 2012). Neurite orientation dispersion (ODI) is a tortuosity measure coupling the intra-neurite space and the extra-neurite space resulting in alignment or dispersion of axons in white matter or axons and dendrites in gray matter (Billiet et al. 2015; Zhang et al. 2012). As described above, each callosal subsection defined for the T1-weighted anatomical scan was transformed into the native space of the diffusion-weighted images to compute NODDI coefficients for these subsections. Moreover, for the evaluation of microstructural integrity of callosal subsections, we also calculated the fractional anisotropy (FA; Basser and Pierpaoli 1996) of each subsection via DTIFIT in FSL (see Fig. 1, top-right).

Statistical analyses

Four dependent variables were used in the present study: FA, INVF, ODI, and ISO, for each of the five subsections of the corpus callosum. The correlations between the dependent variables can be seen in Supplement 1 and Table S1. The statistical analyses were performed assuming a codominant effect for each polymorphism, following the analysis in our previous paper on *PLP1* and *CNTN1* (Ocklenburg et al. 2017). Thus, all genotype groups were analyzed separately. For each of the dependent variables, separate 5×3 repeated-measures ANOVAs were conducted (5×5 for *PLP1* SNPs, as *PLP1* is located on the X chromosome, and therefore has two genotypes for males and three genotypes for females). As myelination and axon density differ between different subsections of the corpus callosum (Aboitiz et al. 1992a, b), we used subsections of the corpus callosum (S1, S2, S3, S4, S5) as the within-subjects variable. Genotype was used the between-subjects variable (Greenhouse–Geisser corrected). Please note that the four dependent variables were partly correlated (see supplementary materials for details). Due to differences in average head size, and therefore possibly brain size, between male (M 57.9, SD 1.5) and female (M 55.4, SD 1.5) participants, $t_{(261)} = 13.5$, $p < 0.001$, we used head size as a covariate in all our analyses. Bonferroni correction was chosen to correct for multiple comparisons and all significant effects are indicated as surviving Bonferroni correction for the number of investigated SNPs. Effect size of significant effects is given as partial η^2. All *t* tests were also corrected for multiple comparisons using Bonferroni correction ($\alpha = 0.01$).

Results

Genotype distributions

For *CNTN1* rs1056019, 13.3% of participants were genotyped homozygous CC, 49.8% were genotyped heterozygous

CT, and 36.9% were genotyped homozygous TT. In our cohort, the minor allele frequency (MAF) for the *CNTN1* rs1056019 was 0.38. The MAF reported for this SNP in dbSNP (https://www.ncbi.nlm.nih.gov/projects/SNP/) is between 0.38 and 0.43. Therefore, the MAF observed in our cohort is in line with what would be expected in the population.

For *PLP1* rs1126707 there were five different genotypes, as this gene is located on the X chromosome (C and T for male individuals, and CC, CT, and TT for female individuals). Therefore, genotype percentages were calculated separately for male and female participants. For males, 28.0% of participants showed the C genotype, and 72.0% showed the T genotype. For females, 6.3% of participants were genotyped homozygous CC, 37.3% of participants were genotyped heterozygous CT, and 56.3% were genotyped homozygous TT. Genotypes could not be determined for five participants due to technical issues. For male participants, the MAF for the *PLP1* rs1126707 was 0.28, and for female participants the MAF for this SNP was 0.25, resulting in a combined MAF of 0.265. The MAF reported for this SNP in dbSNP (https://www.ncbi.nlm.nih.gov/projects/SNP/) is 0.29, and therefore the MAF observed in our cohort is in roughly line with what would be expected in the population.

For *PLP1* rs521895, there were also five different genotypes (A and G for male individuals, and AA, AG, and GG for female individuals). Therefore, genotype percentages were also calculated separately for male and female participants. For males, 30.6% of participants showed the A genotype, and 69.4% showed the G genotype. For females, 8.5% of participants were genotyped homozygous AA, 43.4% were genotyped heterozygous AG, and 48.1% were genotyped homozygous GG. For male participants, the MAF for the *PLP1* rs521895 was 0.31, and for female participants the MAF for this SNP was 0.30, resulting in a combined MAF of 0.305. The MAF reported for this SNP in dbSNP (https://www.ncbi.nlm.nih.gov/projects/SNP/) is 0.38, and therefore the MAF observed in our cohort in roughly line with what would be expected in the population.

Neuroimaging results

Association between genetic variation and neuroimaging results

The results of all analyses are shown in Table 1. Further detailed analyses of significant effects are shown in the following subsections.

CNTN1 rs1056019

We investigated the effects of the *CNTN1* rs1056019 SNP on corpus callosum microstructure by conducting 5 (callosal subsections) × 3 (genotype groups) repeated-measures ANOVAs for each dependent variable, with head size as a covariate. There was a main effect of head size, $F_{(1,242)} = 18.15$, $p < 0.001$, partial $\eta^2 = 0.07$. For all four dependent variables, we found main effects of subsection, all F's$_{(4,968)} > 3.34$, all p's < 0.013, all partial $\eta^2 > 0.01$, but no main effects of genotype, all F's$_{(2,242)} < 2.75$, all p's > 0.07. For one of the NODDI variables, INVF, there was a significant interaction between subsections of the corpus callosum and genotype, surviving Bonferroni correction, $F_{(8,968)} = 3.28$, $p = 0.002$, partial $\eta^2 = 0.03$. For the remaining NODDI variables and FA, there was no significant interaction between subsections of the corpus callosum and genotype, all F's$_{(8,968)} < 2.03$, all p's > 0.05.

To further investigate the interaction between subsection and genotype for INVF, we performed Bonferroni-corrected ($\alpha = 0.01$) independent-samples t tests between the three

Table 1 The effects of genetic variation in the three SNPs on the microstructure of the subsections of the corpus callosum, as determined by the four different dependent variables FA, INVF, ODI, and ISO

Gene	SNP	Imaging measure	ME genotype	ME subsections	Interaction
CNTN1	rs1056019	FA	$p = 0.30$	$\mathbf{p < 0.001; \eta^2 = 0.03}$	$p = 0.05$
		INVF	$p = 0.68$	$\mathbf{p = 0.005; \eta^2 = 0.02}$	$\mathbf{p = 0.002; \eta^2 = 0.03}$
		ODI	$p = 0.07$	$\mathbf{p < 0.001; \eta^2 = 0.03}$	$p = 0.14$
		ISO	$p = 0.58$	$\mathbf{p = 0.013; \eta^2 = 0.01}$	$p = 0.85$
PLP1	rs1126707	FA	$p = 0.75$	$p = 0.12$	$\mathbf{p = 0.01; \eta^2 = 0.03}$
		INVF	$p = 0.67$	$p = 0.26$	$p = 0.48$
		ODI	$p = 0.25$	$p = 0.02$	$p = 0.16$
		ISO	$p = 0.05$	$p = 0.04$	$\mathbf{p = 0.004; \eta^2 = 0.04}$
	rs521895	FA	$p = 0.28$	$p = 0.23$	$\mathbf{p = 0.004; \eta^2 = 0.04}$
		INVF	$p = 0.74$	$p = 0.32$	$p = 0.21$
		ODI	$p = 0.12$	$p = 0.08$	$p = 0.02$
		ISO	$p = 0.07$	$p = 0.04$	$p = 0.07$

Significant effects are shown in bold, after Bonferroni correction and the addition of head size as a covariate. Partial η^2 is given for significant results as a measure of effect size

genotypes (CC, CT, and TT) for each of the subsections of the corpus callosum (S1–S5). Within each subsection of the corpus callosum, no differences between genotypes survived correction for multiple comparisons, all p's > 0.02. However, for the CC genotype, INVF in the S1 subsection was significantly different from all other subsections, all p's < 0.001, and the S5 subsection also showed significantly different INVF from all other subsections, all p's < 0.001. For the CT genotype, all subsections displayed significantly different INVF from each other, all p's < 0.008, except for the S3 and S4 subsections, $p = 0.96$. Similarly, for the TT genotype, a non-significant difference between S3 and S4 subsection INVF was observed ($p = 0.17$), while all other subsections had significant differences in INVF (all p's < 0.006). This interaction effect can be seen in Fig. 2.

PLP1 rs1126707

To investigate the effects of the *PLP1* rs1126707 SNP on corpus callosum microstructure, we conducted 5 × 5 repeated-measures ANOVAs for each dependent variable, with head size as a covariate. There was no main effect of head size, $F_{(1,235)} = 0.83$, $p = 0.37$. For all four dependent variables, we found no significant main effects of subsection, all F's$_{(4,940)} < 3.12$, all p's > 0.02, or genotype, all Fs$_{(4,235)} < 2.46$, all p's > 0.05. There was a significant interaction effect for FA, $F_{(16,940)} = 2.08$, $p = 0.01$, partial $\eta^2 = 0.03$, surviving Bonferroni correction.

We calculated the same t tests for the interaction between genotype and subsection for FA. Within each subsection of the corpus callosum, no differences between genotypes survived correction for multiple comparisons (all p's > 0.014). For the C genotype, FA in all subsections was significantly different to all other subsections, all p's < 0.003, except between the S2 and S4 subsections, $p = 0.99$. This was the same for the T genotype, $p = 0.64$.

For the CC genotype, FA in the S5 subsection was significantly different from all other subsections, all p's < 0.001. No other FA differences were observed between subsections for this genotype. For the CT genotype, FA in all subsections was significantly different from all other subsections, all p's < 0.01, except between the S4 and S1 subsections, $p = 0.14$, and the S4 and S2 subsections, $p = 0.32$. Similarly, for the TT genotype, FA in all subsections was significantly different from all other subsections, all p's < 0.001, except between the S2 and S4 subsections, $p = 0.82$. A full summary of the interaction effect for FA between subsections can be seen in Fig. 3.

For one of the NODDI variables, ISO, there was also a significant interaction between subsections of the corpus callosum and genotype, $F_{(16,940)} = 2.29$, $p = 0.004$, partial $\eta^2 = 0.04$, surviving Bonferroni correction. To further investigate the interaction between subsection and genotype for ISO, we performed Bonferroni-corrected ($\alpha = 0.01$) independent-samples t tests between the five genotypes (A, G, AA, AG, and GG) for each of the subsections of the corpus callosum (S1–S5). Within the S1, S3, S4, and S5 subsections, there were no differences in ISO between all genotypes, all p's > 0.02. However, within the S2 subsection, there was a significant difference in ISO between CC and CT genotypes, $p = 0.002$, as well as CC and TT genotypes ($p = 0.002$).

For the C genotype, ISO in the S1 subsection was significantly different from ISO in all other subsections (all p's < 0.001), except in the S2 subsection, where no significant difference was observed, although it approached significance ($p = 0.011$). ISO in the S2 and S3 subsections was significantly different from ISO in all other sections (all p's < 0.001), except between these two sections ($p = 0.46$).

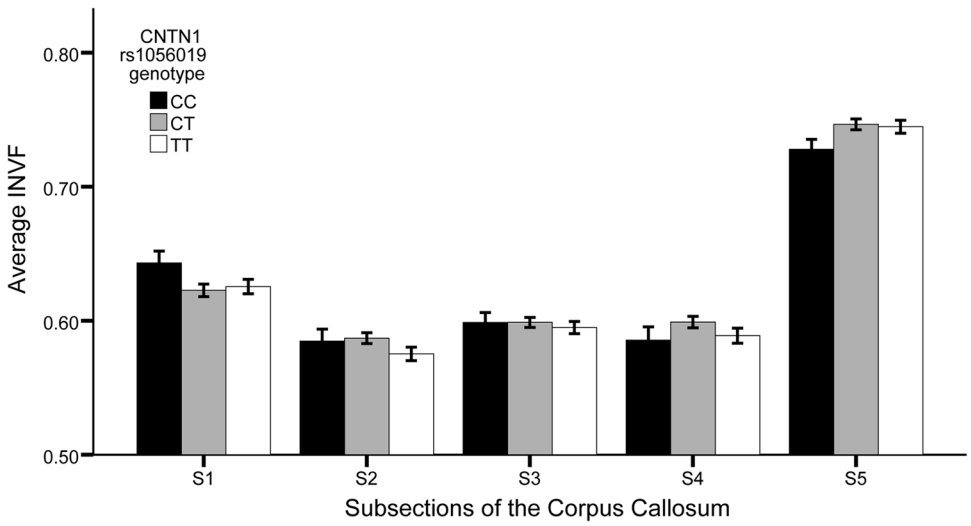

Fig. 2 Average INVF in each subsection of the corpus callosum in relation to *CNTN1* rs1056019 genotype. Error bars show standard error

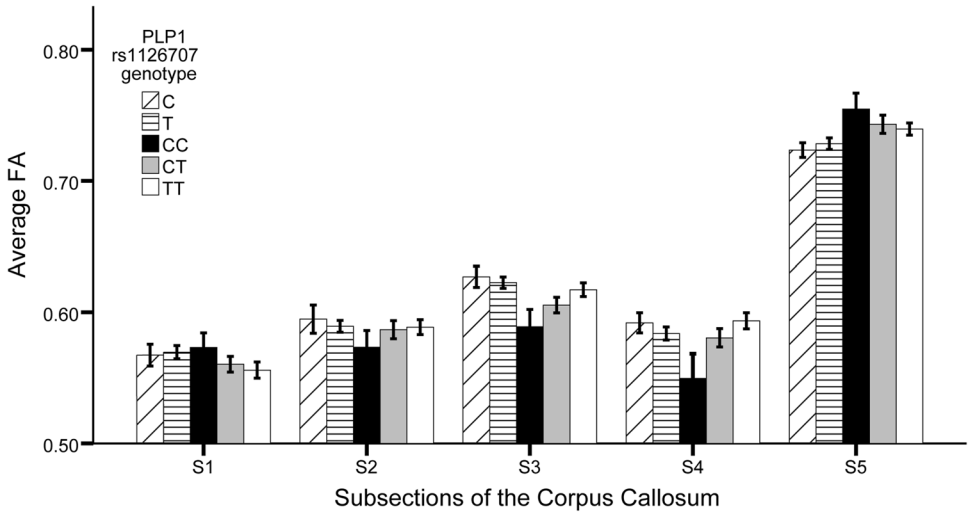

Fig. 3 Average FA in each subsection of the corpus callosum in relation to *PLP1* rs1126707 genotype. Error bars show standard error

For the T genotype, ISO in the S1, S2, and S3 subsections showed a similar pattern of differences to the C genotype: S1 subsection ISO was significantly different from all other subsections (all p's < 0.001), except in the S2 subsection ($p = 0.14$). ISO in the S2 and S3 subsections was also significantly different from all other subsections (all p's < 0.002), except between those two subsections ($p = 0.04$). However, for the T genotype, ISO in the S5 subsection was significantly different from all other subsections (all p's < 0.002), including the S2 subsection, which for the C genotype was not significantly different ($p = 0.11$).

For the CC genotype, ISO in the S5 subsection was significantly different from all other subsections (all p's < 0.005), except for the S3 subsection ($p = 0.53$). However, ISO in the S3 subsection was significantly different to ISO in the S1 and S2 subsections (both p's < 0.007).

For the CT genotype, ISO in the S1 and S4 subsections was significantly different from all other subsections (all p's < 0.001), except between those two sections ($p = 0.65$). For the TT genotype, ISO in the S1 and S4 subsections was significantly different from all other subsections (all p's < 0.003). In the CT and TT genotypes, no other significant differences between subsections were observed. A full summary of the interaction effect for ISO can be seen in Fig. 4.

For the remaining two NODDI variables, INVF and ODI, no significant interaction was found between subsection and genotype (both F's$_{(16,940)} < 1.39$, both p's > 0.16).

PLP1 rs521895

For *PLP1* rs521895, we conducted 5×5 repeated-measures ANOVAs for each dependent variable, with head size as a covariate. There was no main effect of head size, $F_{(1,240)} = 1.26$, $p = 0.26$. For all four dependent variables, we found no significant main effects of subsection (all F's$_{(4,940)} < 2.63$, all p's > 0.04), or genotype (all F's$_{(4,240)} < 2.17$, all p's > 0.07). For the FA measure, there

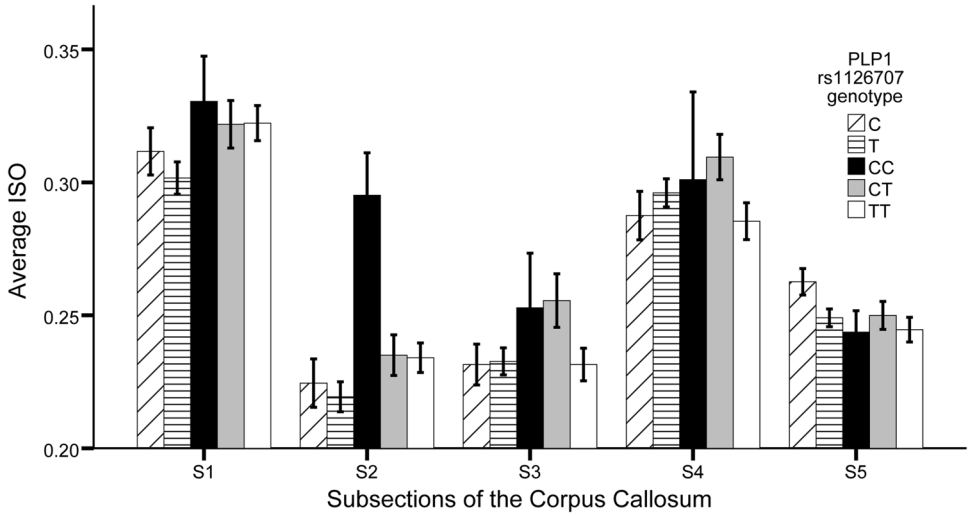

Fig. 4 Average ISO in each subsection of the corpus callosum in relation to *PLP1* rs1126707 genotype. Error bars show standard error

was a significant interaction between subsections of the corpus callosum and genotype that survived Bonferroni correction ($F_{(16,940)} = 2.32$, $p = 0.004$, partial $\eta^2 = 0.04$). For one of the NODDI variables, ODI, the interaction effect approached significance, but did not survive Bonferroni correction ($F_{(16,940)} = 2.01$, $p = 0.02$). For the remaining two NODDI variables, no significant interaction was found between subsection and genotype (both F's$_{(16,940)} < 1.59$, both p's > 0.07).

To further investigate the interaction between subsection and genotype for FA, we performed Bonferroni-corrected ($\alpha = 0.01$) independent-samples t tests between the five genotypes (A, G, AA, AG, and GG) for each of the subsections of the corpus callosum (S1–S5). Within the S1 subsection of the corpus callosum, there was a significant FA difference between GG and AG genotypes, $p = 0.006$. Within all other subsections, there were no differences between A and G, and AA, AG, and GG genotypes.

For both the A and G genotypes, FA in all subsections of the corpus callosum was significantly different from all other subsections (all p's < 0.005), except between the S2 and S4 subsections ($p = 0.95$ and $p = 0.57$, respectively).

For the AA genotype, FA in the S5 subsection was different from all other subsections (all p's < 0.001). FA in the S4 subsection was different from all other subsections (all p's < 0.003), except for the S2 ($p = 0.05$) and S1 subsections ($p = 0.41$). For both of these subsections, FA was significantly different from all other subsections excluding the S4 (all p's < 0.005). FA in the S3 and S2 subsections was not significantly different ($p = 0.36$), but all other subsections showed significantly different FA from the S3 subsection (all p's < 0.003). For the AG genotype, FA in all subsections was significantly different from all other subsections (all p's < 0.004), except between the S2 and S4 subsections ($p = 0.62$). For the GG genotype, FA in both the S3 and S5 subsections was significantly different from all other subsections (all p's < 0.001). No other significant differences in FA between subsections were observed for the GG genotype. A full summary of the interaction effect between subsections of the corpus callosum and genotype for the FA measure can be seen in Fig. 5.

To test whether the inclusion of head size as a covariate influenced the results, we also re-calculated the analysis without head size as a covariate (Supplement 2 and Table S2). Results of all analysis without head size as a covariate are shown in supplementary Table S2. The overall results pattern is almost identical to the analysis with head size as a covariate. Additionally, we also re-calculated our analysis with age as a covariate (Supplement 3 and Figure S1) and only for right-handed participants (Supplement 4).

Discussion

The present study tested the assumption that allelic variations in the myelin genes *PLP1* and *CNTN1* affect the microstructure of the corpus callosum and thus correlate with individual performance in interhemispheric integration (Ocklenburg et al. 2017). Here, we present results on microstructural corpus callosum differences found between cognitively healthy subjects as a function of their *PLP1* and *CNTN1* genotypes. To this end, we used the diffusion neuroimaging technique NODDI to quantify axonal morphology in subsections of the corpus callosum. In line with our hypothesis, we found a double dissociation between gene function and neuroimaging parameters. On the one hand, genetic variation in the myelin-related gene *PLP1* was linked to differences in FA, a measure that encodes microstructural integrity of white matter and has been at least partly linked to myelin structure. On the other hand, genetic variation in the axon guidance related gene *CNTN1*

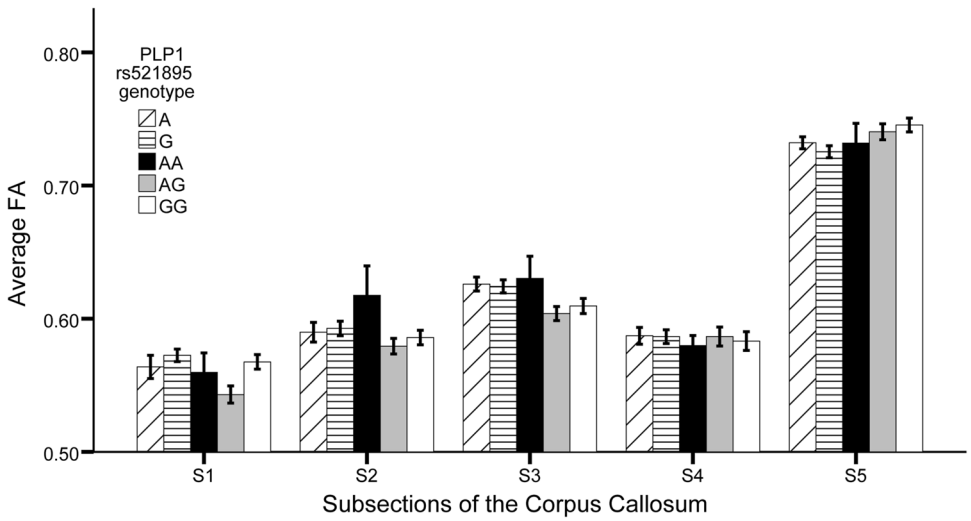

Fig. 5 Average FA in each subsection of the corpus callosum in relation to *PLP1* rs521895 genotype. Error bars show standard error

was associated with axonal density differences between subsections of the corpus callosum as reflected by INVF.

For the general distribution and correlations between NODDI-dependent variables, our neuroimaging data were in line with previous NODDI studies (Mayer et al. 2017). Importantly, the finding that we found a strong association between FA and ODI replicates the findings of a recent microstructure imaging study in mixed-martial artists (Mayer et al. 2017). We used head size as a covariate to control for sex differences. For both *PLP1* SNPs, there was no main effect of head size, but there was for the *CNTN1* SNP. To control for possible confounding effects of age, we re-ran the ANOVAs for all four significant dependent variables. There was no significant effect of age or any change in the overall results pattern when age was included in the analysis.

For the *CNTN1* rs1056019 SNP, the main finding was that we observed a significant interaction between genotype and corpus callosum subsection for INVF, but not for FA or the other NODDI variables. Although there were no differences between the three genotypes (CC, CT, and TT) within each subsection of the corpus callosum that survived correction for multiple comparisons, we did find that for the CT and TT genotypes, INVF in S2 was different from all other subsections, whereas this was not the case for the CC genotype. The NODDI measure INVF is a measure of neurite density, and represents the amount of symmetric diffusion caused by the restriction of water molecules within the membranes of neurites (Jespersen et al. 2010, 2012; Zhang et al. 2012). INVF is likely to represent the proportion of axons in white matter, i.e., in the corpus callosum. The interaction effect that we found between genotype and corpus callosum subsections suggests that variation in *CNTN1* specifically correlates with axon density, but not axon or CSF dispersion.

The finding that genetic variation in *CNTN1* did differentially affect corpus callosum subsections is in line with the finding that myelination and axon density differ between different subsections of the corpus callosum (Aboitiz et al. 1992a, b). Rs1056019 leads to the synonymous exchange of an asparagine in *CNTN1*. Although the specific effect of this SNP on *CNTN1* gene function remains unclear, our finding is well in line with previous literature on *CNTN1* gene function in general. *CNTN1* is located on chromosome 12 at 12q11–q12 and is a member of the immunoglobulin (Ig) gene family. It encodes contactin-1, a glycosylphosphatidylinositol-anchored neuronal membrane protein that functions as a cell adhesion molecule (Berglund and Ranscht 1994). It has been shown to modulate axon connections and neurogenesis during central nervous system development (Bizzoca et al. 2012), which could explain why variation in this gene specifically affects the NODDI variable INVF. Moreover, it has been shown that a complex between contactin-1 and the protein tyrosine phosphatase PTPRZ modulates the development and differentiation of oligodendrocyte precursor cells (Lamprianou et al. 2011).

For *PLP1*, we found that both SNPs show significant association with FA. For the *PLP1* rs1126707 SNP, the main finding was that we observed a significant interaction between genotype and corpus callosum subsection for FA. While no differences in the relationship between genetic variation in *PLP1* and FA in callosal subsections were found between the two genotypes in male participants, the CC genotype stood out in female participants, as it seemed to show less differentiation of FA between different callosal subsections. Comparable to the *PLP1* rs1126707 SNP, we also found a significant interaction between genotype and corpus callosum subsection FA for the *PLP1* rs521895 SNP. Here, we found that for subsection S1, the most anterior part of the corpus callosum, there was a significant FA difference between females with the GG and AG genotypes that survived correction for multiple comparisons. Moreover, comparable to the CC genotype for the *PLP1* rs1126707 SNP, the rare homozygous AA genotype stood out in female participants, as it seemed to show less differentiation of FA between different callosal subsections than the other genotypes. It should be noted that both *CNTN1* and *PLP1* genes have complex phenotypes, and so we cannot know for certain whether there are any confounding effects of population substructure and stratification, which may result in exaggerated effect sizes.

The exact functional consequences of the two associated *PLP1* SNPs also remain elusive, but our result that variation in *PLP1* affected mainly FA is in line with the general gene function attributed to *PLP1*. *PLP1* is located on the X chromosome at Xq22.2. It encodes a transmembrane proteolipid protein that is one of the major components of myelin (Martínez-Montero et al. 2013; Wight 2017; Woodward and Malcolm 1999). Proteolipid protein has been shown to be involved in the early stages of axon–oligodendrocyte interaction and to modulate how the axon is wrapped (Yool et al. 2001). Duplications or point mutations in *PLP1* are known to be causative of Pelizaeus–Merzbacher disease (PMD), a classic example of a hypomyelinating leukodystrophy and the allelic spastic paraplegia 2 (SPG2). Pelizaeus–Merzbacher disease is characterized by nystagmus, hypotonia, and severe motor deficits (Inoue 2005; Martínez-Montero et al. 2013). Different types of mutations in *PLP1* are suspected to have different impacts on the oligodendrocyte lineage. In most PMD children, the amount of white matter is reduced in volume and can be readily seen as thinness of the corpus callosum or general decrease in myelination (Plecko et al. 2003). In line with these findings, patients with Pelizaeus–Merzbacher disease typically show atrophy of the corpus callosum (Sarret et al. 2016). As mentioned above, FA in white matter is thought to reflect myelin, axon diameter and packing density, axon permeability, and fiber geometry

(Beaulieu 2002; Mädler et al. 2008; Mori and Zhang 2006; Zatorre et al. 2012). As *PLP1* encodes a major component of myelin, it is conceivable that it modulates FA by affecting myelin structure. This idea is supported by a recent DTI study in a mouse model for Pelizaeus–Merzbacher disease that showed a significant reduction of FA in the corpus callosum of *PLP1* transgenic mice (Ruest et al. 2011).

Our finding that genetic variation in *CNTN1* and *PLP1* affects corpus callosum microstructure is also in line with the finding of our previous study showing a relevance of genetic variation in *CNTN1* and *PLP1* for corpus callosum function (Ocklenburg et al. 2017). In this study, we investigated whether performance in the Banich–Belger Task was also modulated by genetic variation in *CNTN1* and *PLP1*. In this task, arrays of three letters are presented to participants in a triangular formation. Two letters are placed above a fixation point, with one letter presented in the left visual field (LVF) and the other in the right visual field (RVF). The third target letter is placed below the fixation point, in either the LVF or RVF. Participants have to indicate whether the target letter matches one of the other two letters based on name identity, or physical identity. In the name identity task, participants have to decide whether the target letter (in lowercase) has the same name value as one of the other two letters (in uppercase). In the physical identity task, participants have to decide whether the target letter has the same physical form as one of the two other letters (all uppercase). Generally, participants are faster at the name identity task when the target letter is in the contralateral visual field (across trials), but are faster at the physical identity task when the target letter is in the ipsilateral visual field (Banich and Belger 1990; Ocklenburg et al. 2017). Thus, the Banich–Belger task assesses interhemispheric integration, via the corpus callosum. In our previous study, no differences between *CNTN1* rs1056019 genotype groups were found during the physical identity condition of the Banich–Belger task. However, during the more complex name identity condition, the CC group was more accurate during within trials, while both the CT and TT groups were more accurate during across trials. We argued that the CC genotype group likely had less efficient interhemispheric transfer via the corpus callosum than CT and TT groups (Ocklenburg et al. 2017). This is in line with findings of the present study. In the present study, it was also the CC genotype group that stood out from the CT and TT groups. In contrast to the other two genotypes, individuals with the CC genotype showed a lower frequency of significant differences between callosal subsections, arguing for a less pronounced axonal density differentiation of callosal subsections, which could potentially lead to the less efficient interhemispheric integration observed in our behavioral study with the Banich–Belger task.

In addition to the FA effects, we also observed a significant interaction between *PLP1* rs1126707 genotype and corpus callosum subsection for ISO. As outlined above, ISO reflects the amount of isotropic diffusion likely to be found in the cerebrospinal fluid of gray and white matter regions. We can only speculate why this measure is linked to genetic variation in *PLP1*, but has been shown that certain mutations in *PLP1* can lead to atrophy of the corpus callosum (Sarret et al. 2016). As a thinner corpus callosum would lead to less tissue dispersion, this would likely result in higher ISO values. Moreover, as shown in Table S1 (see supplementary materials), FA and ISO were correlated negatively for all five callosal subsections. This makes sense as ISO reflects isotropic diffusion (as in cerebrospinal fluid), while FA reflects anisotropic diffusion (as in tissue).

As this study represents the first neurogenetic study on the relation between genetic variation in *PLP1* and *CNTN1* and corpus callosum microstructure, it was explorative in nature. Despite that, it offers several interesting suggestions for the design of future studies. Obviously, independent replication of our results in larger cohorts would be essential to validate our findings (Flint and Munafò 2013). This is especially the case as in a recent analysis by the ENIGMA consortium, no associations between genetic variation in one of 15 candidate SNP's and white matter microstructure remained significant after multiple-testing correction (Jahanshad et al. 2017).

In addition, it would be particularly interesting to assess corpus callosum microstructure in patient cohorts with *PLP1* mutations, e.g., patients with Pelizaeus–Merzbacher disease (Wight 2017), to get a better understanding of the functional effects of *PLP1* on corpus callosum microstructure. In healthy cohorts, extended neuroimaging, e.g., NODDI in other key white matter structures such as the arcuate fasciculus or uncinate fasciculus (Ocklenburg et al. 2013) would be interesting to get a more detailed picture of the effects of genetic variation in *PLP1* and *CNTN1* on white matter brain structure. In addition to NODDI imaging, other advanced white matter neuroimaging techniques would also be interesting to use in *PLP1* and *CNTN1* neurogenetics studies, e.g., estimation of myelin water fraction (Alonso-Ortiz et al. 2015; Nam et al. 2015).

The current study represents the first neurogenetic study on corpus callosum microstructure using NODDI. Interestingly, we found a double dissociation between gene function and neuroimaging variables. Our results suggest that genetic variation in the myelin-related gene *PLP1* impacts white matter microstructure in the corpus callosum, as reflected by FA. As described above, FA does not exclusively reflect myelin structure, but it does so to a larger extent than INVF, which reflects neurite density, and specifically axonal density in the corpus callosum. Given the clear functional role of *PLP1* in encoding one of the major myelin proteins, it is conceivable that variation in this gene affects FA by affecting myelin structure. In contrast, genetic variation in the

axon guidance related gene *CNTN1* impacts axonal density in the corpus callosum, as indicated by INVF.

Acknowledgements This work was funded by Grants from the Deutsche Forschungsgemeinschaft (DFG) Gu227/16-1, GE2777/2-1 and BE4045/26-1.

Compliance with ethical standards

Conflict of interest The authors declare that they have no conflict of interest.

References

Aboitiz F, Scheibel AB, Fisher RS, Zaidel E (1992a) Fiber composition of the human corpus callosum. Brain Res 598(1–2):143–153

Aboitiz F, Scheibel AB, Zaidel E (1992b) Morphometry of the Sylvian fissure and the corpus callosum, with emphasis on sex differences. Brain J Neurol 115(Pt 5):1521–1541

Alonso-Ortiz E, Levesque IR, Pike GB (2015) MRI-based myelin water imaging: a technical review. Magn Reson Med 73(1):70–81. https://doi.org/10.1002/mrm.25198

Banich MT, Belger A (1990) Interhemispheric interaction: how do the hemispheres divide and conquer a task? Cortex J Devot Stud Nerv Syst Behav 26(1):77–94

Basser PJ, Pierpaoli C (1996) Microstructural and physiological features of tissues elucidated by quantitative-diffusion-tensor MRI. J Magn Reson Ser B 111(3):209–219

Beaulieu C (2002) The basis of anisotropic water diffusion in the nervous system—a technical review. NMR Biomed 15(7–8):435–455. https://doi.org/10.1002/nbm.782

Behrens TEJ, Berg HJ, Jbabdi S, Rushworth MFS, Woolrich MW (2007) Probabilistic diffusion tractography with multiple fibre orientations: what can we gain? NeuroImage 34(1):144–155. https://doi.org/10.1016/j.neuroimage.2006.09.018

Berglund EO, Ranscht B (1994) Molecular cloning and in situ localization of the human contactin gene (CNTN1) on chromosome 12q11–q12. Genomics 21(3):571–582. https://doi.org/10.1006/geno.1994.1316

Billiet T, Vandenbulcke M, Mädler B, Peeters R, Dhollander T, Zhang H, Emsell L (2015) Age-related microstructural differences quantified using myelin water imaging and advanced diffusion MRI. Neurobiol Aging 36(6):2107–2121. https://doi.org/10.1016/j.neurobiolaging.2015.02.029

Bizzoca A, Corsi P, Polizzi A, Pinto MF, Xenaki D, Furley AJW, Gennarini G (2012) F3/Contactin acts as a modulator of neurogenesis during cerebral cortex development. Dev Biol 365(1):133–151. https://doi.org/10.1016/j.ydbio.2012.02.011

Boiko T, Winckler B (2006) Myelin under construction—teamwork required. J Cell Biol 172(6):799–801. https://doi.org/10.1083/jcb.200602101

Caminiti R, Ghaziri H, Galuske R, Hof PR, Innocenti GM (2009) Evolution amplified processing with temporally dispersed slow neuronal connectivity in primates. Proc Natl Acad Sci USA 106(46):19551–19556. https://doi.org/10.1073/pnas.0907655106

Clarke JM, Zaidel E (1994) Anatomical-behavioral relationships: corpus callosum morphometry and hemispheric specialization. Behav Brain Res 64(1–2):185–202

Czopka T, Holst A von, Ffrench-Constant C, Faissner A (2010) Regulatory mechanisms that mediate tenascin C-dependent inhibition of oligodendrocyte precursor differentiation. J Neurosci 30(37):12310–12322. https://doi.org/10.1523/JNEUROSCI.4957-09.2010

Daducci A, Canales-Rodríguez EJ, Zhang H, Dyrby TB, Alexander DC, Thiran J-P (2015) Accelerated microstructure imaging via convex optimization (AMICO) from diffusion MRI data. NeuroImage 105:32–44. https://doi.org/10.1016/j.neuroimage.2014.10.026

Dale AM, Fischl B, Sereno MI (1999) Cortical surface-based analysis. I. Segmentation and surface reconstruction. NeuroImage 9(2):179–194. https://doi.org/10.1006/nimg.1998.0395

DeCarli C, Murphy DG, Tranh M, Grady CL, Haxby JV, Gillette JA, Rapoport SI (1995) The effect of white matter hyperintensity volume on brain structure, cognitive performance, and cerebral metabolism of glucose in 51 healthy adults. Neurology 45(11):2077–2084

Fabri M, Pierpaoli C, Barbaresi P, Polonara G (2014) Functional topography of the corpus callosum investigated by DTI and fMRI. World J Radiol 6(12):895–906. https://doi.org/10.4329/wjr.v6.i12.895

Fischl B, Sereno MI, Dale AM (1999) Cortical surface-based analysis. II: Inflation, flattening, and a surface-based coordinate system. NeuroImage 9(2):195–207. https://doi.org/10.1006/nimg.1998.0396

Flint J, Munafò MR (2013) Candidate and non-candidate genes in behavior genetics. Curr Opin Neurobiol 23(1):57–61. https://doi.org/10.1016/j.conb.2012.07.005

Froeling M, Tax CMW, Vos SB, Luijten PR, Leemans A (2017) "MASSIVE" brain dataset: multiple acquisitions for standardization of structural imaging validation and evaluation. Magn Reson Med 77(5):1797–1809. https://doi.org/10.1002/mrm.26259

Garde E, Mortensen EL, Krabbe K, Rostrup E, Larsson HB (2000) Relation between age-related decline in intelligence and cerebral white-matter hyperintensities in healthy octogenarians: a longitudinal study. Lancet 356(9230):628–634. https://doi.org/10.1016/S0140-6736(00)02604-0

Ge Y, Grossman RI, Babb JS, Rabin ML, Mannon LJ, Kolson DL (2002) Age-related total gray matter and white matter changes in normal adult brain. Part I: Volumetric MR imaging analysis. Am J Neuroradiol 23(8):1327–1333

Genç E, Ocklenburg S, Singer W, Güntürkün O (2015) Abnormal interhemispheric motor interactions in patients with callosal agenesis. Behav Brain Res 293:1–9. https://doi.org/10.1016/j.bbr.2015.07.016

Genç E, Fraenz C, Schlüter C, Friedrich P, Hossiep R, Voelkle MC, Ling JM, Güntürkün O, Jung RE (2018) Diffusion markers of dendritic density and arborization in gray matter predict differences in intelligence. Nat Commun 9:1905. https://doi.org/10.1038/s41467-018-04268-8

Grussu F, Schneider T, Tur C, Yates RL, Tachrount M, Ianuş A, Yiannakas MC, Newcombe J, Zhang H, Alexander DC, DeLuca GC, Gandini Wheeler-Kingshott CAM (2017) Neurite dispersion: a new marker of multiple sclerosis spinal cord pathology? Ann Clin Transl Neurol 4(9):663–679. https://doi.org/10.1002/acn3.445

Hofer S, Frahm J (2006) Topography of the human corpus callosum revisited—comprehensive fiber tractography using diffusion tensor magnetic resonance imaging. NeuroImage 32(3):989–994. https://doi.org/10.1016/j.neuroimage.2006.05.044

Inoue K (2005) PLP1-related inherited dysmyelinating disorders: Pelizaeus–Merzbacher disease and spastic paraplegia type 2. Neurogenetics 6(1):1–16. https://doi.org/10.1007/s10048-004-0207-y

Jahanshad N, Ganjgahi H, Bralten J, den Braber A, Faskowitz J, Knodt A, Sprooten E (2017) Do candidate genes affect the brain's white matter microstructure? Large-scale evaluation of 6165 diffusion MRI scans. bioRxiv. https://doi.org/10.1101/107987

Jespersen SN, Bjarkam CR, Nyengaard JR, Chakravarty MM, Hansen B, Vosegaard T, Vestergaard-Poulsen P (2010) Neurite density from magnetic resonance diffusion measurements at ultrahigh

field: comparison with light microscopy and electron microscopy. NeuroImage 49(1):205–216. https://doi.org/10.1016/j.neuroimage.2009.08.053

Jespersen SN, Leigland LA, Cornea A, Kroenke CD (2012) Determination of axonal and dendritic orientation distributions within the developing cerebral cortex by diffusion tensor imaging. IEEE Trans Med Imaging 31(1):16–32. https://doi.org/10.1109/TMI.2011.2162099

Lamprianou S, Chatzopoulou E, Thomas J-L, Bouyain S, Harroch S (2011) A complex between contactin-1 and the protein tyrosine phosphatase PTPRZ controls the development of oligodendrocyte precursor cells. Proc Natl Acad Sci USA 108(42):17498–17503. https://doi.org/10.1073/pnas.1108774108

Le Bihan D (2003) Looking into the functional architecture of the brain with diffusion MRI. Nat Rev Neurosci 4(6):469–480. https://doi.org/10.1038/nrn1119

Mädler B, Drabycz SA, Kolind SH, Whittall KP, MacKay AL (2008) Is diffusion anisotropy an accurate monitor of myelination? Correlation of multicomponent T2 relaxation and diffusion tensor anisotropy in human brain. Magn Reson Imaging 26(7):874–888. https://doi.org/10.1016/j.mri.2008.01.047

Martínez-Montero P, Muñoz-Calero M, Vallespín E, Campistol J, Martorell L, Ruiz-Falcó MJ, Molano J (2013) PLP1 gene analysis in 88 patients with leukodystrophy. Clin Genet 84(6):566–571. https://doi.org/10.1111/cge.12103

Mayer AR, Ling JM, Dodd AB, Meier TB, Hanlon FM, Klimaj SD (2017) A prospective microstructure imaging study in mixed-martial artists using geometric measures and diffusion tensor imaging: methods and findings. Brain Imaging Behav 11(3):698–711. https://doi.org/10.1007/s11682-016-9546-1

Mori S, Zhang J (2006) Principles of diffusion tensor imaging and its applications to basic neuroscience research. Neuron 51(5):527–539. https://doi.org/10.1016/j.neuron.2006.08.012

Nam Y, Lee J, Hwang D, Kim D-H (2015) Improved estimation of myelin water fraction using complex model fitting. NeuroImage 116:214–221. https://doi.org/10.1016/j.neuroimage.2015.03.081

Ocklenburg S, Hugdahl K, Westerhausen R (2013) Structural white matter asymmetries in relation to functional asymmetries during speech perception and production. NeuroImage 83:1088–1097. https://doi.org/10.1016/j.neuroimage.2013.07.076

Ocklenburg S, Gerding WM, Arning L, Genç E, Epplen JT, Güntürkün O, Beste C (2017) Myelin genes and the corpus callosum: proteolipid protein 1 (PLP1) and Contactin 1 (CNTN1) gene variation modulates interhemispheric integration. Mol Neurobiol 54:7908–7916. https://doi.org/10.1007/s12035-016-0285-5

Oldfield RC (1971) The assessment and analysis of handedness: the Edinburgh inventory. Neuropsychologia 9(1):97–113

Pierpaoli C, Basser PJ (1996) Toward a quantitative assessment of diffusion anisotropy. Magn Reson Med 36(6):893–906

Plecko B, Stöckler-Ipsiroglu S, Gruber S, Mlynarik V, Moser E, Simbrunner J. Prayer D (2003) Degree of hypomyelination and magnetic resonance spectroscopy findings in patients with Pelizaeus Merzbacher phenotype. Neuropediatrics 34(3):127–136. https://doi.org/10.1055/s-2003-41276

Rosas HD, Lee SY, Bender AC, Zaleta AK, Vangel M, Yu P, Hersch SM (2010) Altered white matter microstructure in the corpus callosum in Huntington's disease: implications for cortical "disconnection". NeuroImage 49(4):2995–3004. https://doi.org/10.1016/j.neuroimage.2009.10.015

Ruest T, Holmes WM, Barrie JA, Griffiths IR, Anderson TJ, Dewar D, Edgar JM (2011) High-resolution diffusion tensor imaging of fixed brain in a mouse model of Pelizaeus–Merzbacher disease: comparison with quantitative measures of white matter pathology. NMR Biomed 24(10):1369–1379. https://doi.org/10.1002/nbm.1700

Sarret C, Lemaire J-J, Tonduti D, Sontheimer A, Coste J, Pereira B, Boespflug-Tanguy O (2016) Time-course of myelination and atrophy on cerebral imaging in 35 patients with PLP1-related disorders. Dev Med Child Neurol 58(7):706–713. https://doi.org/10.1111/dmcn.13025

Schmahmann JD, Smith EE, Eichler FS, Filley CM (2008) Cerebral white matter: neuroanatomy, clinical neurology, and neurobehavioral correlates. Ann N Y Acad Sci 1142:266–309. https://doi.org/10.1196/annals.1444.017

Sepehrband F, Alexander DC, Kurniawan ND, Reutens DC, Yang Z (2016) Towards higher sensitivity and stability of axon diameter estimation with diffusion-weighted MRI. NMR Biomed 29(3):293–308. https://doi.org/10.1002/nbm.3462

Skoog I, Berg S, Johansson B, Palmertz B, Andreasson LA (1996) The influence of white matter lesions on neuropsychological functioning in demented and non-demented 85-year-olds. Acta Neurol Scand 93(2–3):142–148

Suárez R, Gobius I, Richards LJ (2014) Evolution and development of interhemispheric connections in the vertebrate forebrain. Front Hum Neurosci 8:497. https://doi.org/10.3389/fnhum.2014.00497

Tariq M, Schneider T, Alexander DC, Gandini Wheeler-Kingshott CA, Zhang H (2016) Bingham-NODDI: mapping anisotropic orientation dispersion of neurites using diffusion MRI. NeuroImage 133:207–223. https://doi.org/10.1016/j.neuroimage.2016.01.046

van der Knaap LJ, van der Ham IJM (2011) How does the corpus callosum mediate interhemispheric transfer? A review. Behav Brain Res 223(1):211–221. https://doi.org/10.1016/j.bbr.2011.04.018

van der Knaap M, Valk J, Barkhof F (2005) Magnetic resonance of myelination and myelin disorders, 3rd edn. Springer, Berlin

Westerhausen R, Hugdahl K (2008) The corpus callosum in dichotic listening studies of hemispheric asymmetry: a review of clinical and experimental evidence. Neurosci Biobehav Rev 32(5):1044–1054. https://doi.org/10.1016/j.neubiorev.2008.04.005

Wight PA (2017) Effects of intron 1 sequences on human PLP1 expression: implications for PLP1-related disorders. ASN Neuro 9(4):17590914–17720583. https://doi.org/10.1177/1759091417720583

Woodward K, Malcolm S (1999) Proteolipid protein gene: Pelizaeus–Merzbacher disease in humans and neurodegeneration in mice. Trends Genet 15(4):125–128

Yool DA, Klugmann M, McLaughlin M, Vouyiouklis DA, Dimou L, Barrie JA, Griffiths IR (2001) Myelin proteolipid proteins promote the interaction of oligodendrocytes and axons. J Neurosci Res 63(2):151–164. https://doi.org/10.1002/1097-4547(20010115)63:2%3C151::AID-JNR1007%3E3.0.CO;2-Y

Zatorre RJ, Fields RD, Johansen-Berg H (2012) Plasticity in gray and white: neuroimaging changes in brain structure during learning. Nat Neurosci 15(4):528–536. https://doi.org/10.1038/nn.3045

Zhang H, Schneider T, Wheeler-Kingshott CA, Alexander DC (2012) NODDI: practical in vivo neurite orientation dispersion and density imaging of the human brain. NeuroImage 61(4):1000–1016. https://doi.org/10.1016/j.neuroimage.2012.03.072